



Spin-orbit coupling dependent energy transfer in luminescent nonanuclear Yb-Gd / Yb-Lu clusters

Shun Omagari^a, Takayuki Nakanishi^{b,*}, Yuichi Kitagawa^b, Tomohiro Seki^b, Koji Fushimi^b, Hajime Ito^b, Andries Meijerink^c, Yasuchika Hasegawa^{b,*}

^a Graduate School of Chemical Sciences and Engineering, Hokkaido University, N13 W8, Kita-Ku, Sapporo, Hokkaido 060-8628, Japan

^b Faculty of Engineering, Hokkaido University, N13 W8, Kita-Ku, Sapporo, Hokkaido 060-8628, Japan

^c Debye Institute, Department of Chemistry, Utrecht University, Princetonplein 5, 3584 CC Utrecht, The Netherlands

ARTICLE INFO

Keywords:

Lanthanide complexes

Lanthanide clusters

Energy transfer

Spin-orbit coupling

ABSTRACT

In luminescent lanthanide (Ln(III)) complexes, the yield and the lifetime of triplet excited state of organic ligands are crucial factors that affect the ligands-to-Ln(III) energy transfer efficiency. Such factors are dependent on spin-orbit coupling induced by the Ln(III) ions that mixes different multiplicity states through heavy atom and paramagnetic effects. We investigated the role of these effects on the energy transfer efficiency in synthesized nonanuclear Yb-Gd / Yb-Lu clusters ($[\text{Ln}_9(\mu\text{-OH})_{10}(\text{butyl salicylate})_{16}]\text{NO}_3$, $\text{Ln}_9 = \text{Yb}_n\text{Gd}_{9-n}$ or $\text{Yb}_n\text{Lu}_{9-n}$, $n = 0, 1, 3, 7$, and 9). Based on the intensity of the fluorescence and phosphorescence of the ligands, the spin-orbit coupling strength was in the order of $\text{Yb(III)} > \text{Gd(III)} > \text{Lu(III)}$. Various photophysical processes affecting the energy transfer efficiency in $\text{Yb}_n\text{Gd}_{9-n}$ and $\text{Yb}_n\text{Lu}_{9-n}$ clusters are discussed from the perspective of spin-orbit coupling and give insight in how to optimize energy transfer efficiencies.

1. Introduction

Over the past two decades, trivalent lanthanide (Ln(III)) complexes have been extensively studied for their unique spectroscopic properties such as high-chromaticity emission and long emission lifetimes that are advantageous for application to organic light-emitting diodes (OLEDs), [1,2] bioimaging, [3,4] and spectral converters. [5,6] Light-harvesting organic ligands play a major role in photosensitization of Ln(III) ions (photosensitized energy transfer, PSET), which are otherwise poor absorbers of light. [7] The mechanism of photosensitization is depicted in Fig. 1. When organic ligands absorb a photon, a transition from the singlet ground state (S_0) to the singlet excited state (S_1) occurs. Intersystem crossing (ISC) to the triplet excited state (T_1) immediately follows after the transition. Energy transfer to a Ln(III) ion typically proceeds from the T_1 state of the organic ligand. [8,9] Therefore, the efficiency of the PSET is high for Ln(III) complexes with fast $S_1 \rightarrow T_1$ ISC and slow $T_1 \rightarrow S_0$ relaxation.

While $S_1 \rightarrow T_1$ ISC and $T_1 \rightarrow S_0$ relaxation are spin-forbidden processes, they can become partially allowed processes by spin-orbit coupling (SOC). [10] The SOC in Ln(III) complexes is strong due to 1) large effective nuclear charge of Ln(III) ions (the “heavy atom effect”), and 2) the spin and orbital angular momentum of 4f-electrons (the “paramagnetic effect”). As a result, $S_1 \rightarrow T_1$ ISC rate in Ln(III) complexes is

assumed to be fast and ranges anywhere between 10^7 to 10^{10} s^{-1} . [11–13] Reports by Tobita [11] and Guldi [13] both showed that the difference in SOC arises predominantly from the paramagnetic effect rather than the heavy atom effect in the lanthanide series. For example, Gd(III) complex with methyl salicylate ligands showed an order of magnitude larger $S_1 \rightarrow T_1$ ISC and $T_1 \rightarrow S_0$ relaxation rates compared to Lu(III) complex despite Lu(III) being the heavier atom. Guldi and his coworkers further demonstrated that both $S_1 \rightarrow T_1$ ISC and $T_1 \rightarrow S_0$ relaxation rates are roughly proportional to the magnetic moment of the lanthanides. [13]

In terms of raising the PSET efficiency, we suggest that there is an optimum strength of SOC. PSET efficiency η_{sens} can be expressed as the product of $S_1 \rightarrow T_1$ ISC efficiency η_{ISC} and $T_1 \rightarrow \text{Ln}$ energy transfer efficiency $\eta_{T_1 \rightarrow \text{Ln}}$:

$$\eta_{\text{sens}} = \eta_{\text{ISC}} \times \eta_{T_1 \rightarrow \text{Ln}} = \frac{k_{\text{ISC}}}{k_{r, S_1} + k_{nr, S_1} + k_{\text{ISC}}} \times \frac{k_{T_1 \rightarrow \text{Ln}}}{k_{r, T_1} + k_{nr, T_1} + k_{T_1 \rightarrow \text{Ln}}}$$

where k_{ISC} , $k_{T_1 \rightarrow \text{Ln}}$, k_r , and k_{nr} are $S_1 \rightarrow T_1$ ISC, $T_1 \rightarrow \text{Ln}$ energy transfer, radiative, and nonradiative rate constants, respectively. Since SOC mixes different multiplicity states, k_{ISC} as well as k_{r, T_1} and k_{nr, T_1} are raised in the presence of strong SOC. From the equation above, strong SOC

* Corresponding authors.

E-mail addresses: nakanishi@eng.hokudai.ac.jp (T. Nakanishi), hasegaway@eng.hokudai.ac.jp (Y. Hasegawa).

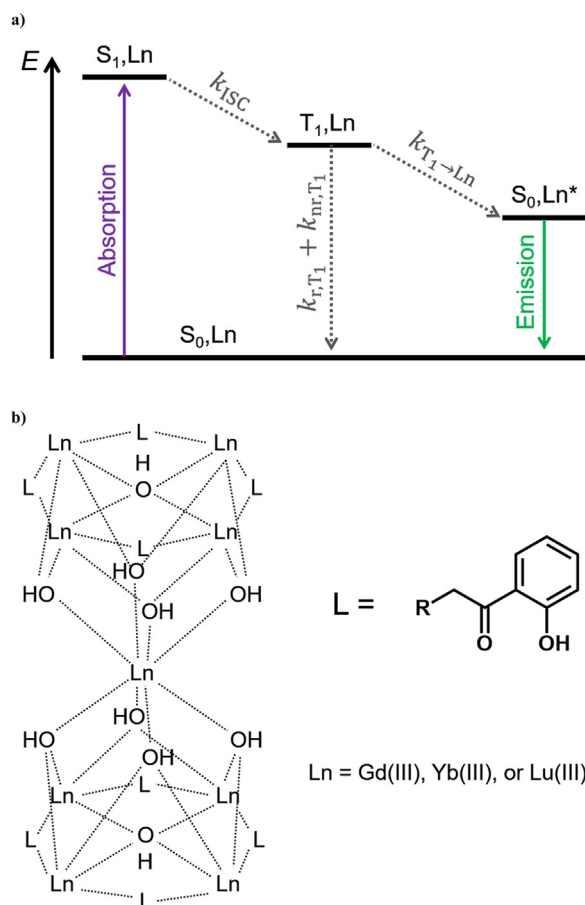


Fig. 1. a) Energy diagram of typical Ln(III) complexes showing various photophysical processes. S_0 : ligand singlet ground state, S_1 : ligand singlet excited state, T_1 : ligand triplet excited state, Ln: ground state Ln(III) ion, Ln^* : excited state Ln(III) ion. ISC: Intersystem crossing, ET: $T_1 \rightarrow Ln$ energy transfer. b) Nonanuclear Ln(III) clusters with ester salicylate ligands.

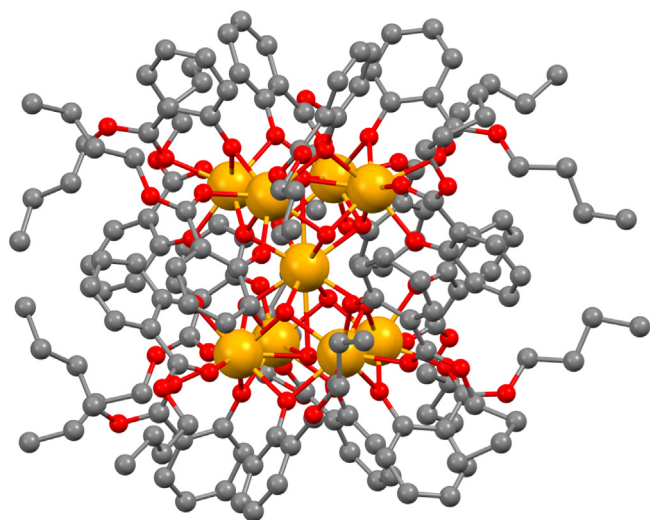


Fig. 2. Crystal structure of Yb_9 cluster. Orange: Yb atoms, red: oxygen atoms, and grey: carbon atoms. Hydrogen atoms as well as the random disorder of the butyl chains are omitted for clarity.

leads to high η_{ISC} but low $\eta_{T_1 \rightarrow Ln}$ while weak SOC leads to low η_{ISC} but high $\eta_{T_1 \rightarrow Ln}$. The opposite action of SOC on these two efficiencies determines the overall η_{sens} and indicates there is an optimum SOC to maximize the product of η_{ISC} and $\eta_{T_1 \rightarrow Ln}$. In order to experimentally

Table 1

Continuous shape measure calculation results for Gd_9 , Yb_9 , and Lu_9 clusters.

	Gd_9 cluster ^a		Yb_9 cluster		Lu_9 cluster	
	8-TDH	8-SAP	8-TDH	8-SAP	8-TDH	8-SAP
Ln1	2.976	4.725	2.573	4.578	2.565	4.455
Ln2	2.836	4.813	2.545	4.546	2.481	4.633
Ln3	2.704	4.588	2.413	4.776	2.447	4.622
Ln4	2.513	4.822	2.404	4.623	2.400	4.507
Ln5	2.976	4.725	2.573	4.578	2.565	4.455
Ln6	2.836	4.813	2.545	4.546	2.481	4.633
Ln7	2.704	4.588	2.413	4.776	2.447	4.622
Ln8	2.513	4.822	2.404	4.623	2.400	4.507
Ln9 ^b	2.481	0.082	2.396	0.077	2.371	0.105

^a Taken from reference [15].

^b Center Ln(III) ion.

observe this effect, we focused on nonanuclear Ln(III) clusters (Fig. 1). [14,15] Nonanuclear Ln(III) clusters are polynuclear Ln(III) complexes composed of nine “clustered” Ln(III) ions and sixteen surrounding ester salicylate ligands. The clusters allow control of SOC by mixing different Ln(III) ions without significantly distorting the structure. Yb(III), Gd(III), and Lu(III) ions were chosen for this work. The Yb(III) ion with its two-level 4f-states ($^2F_{7/2}$ and $^2F_{5/2}$ states) is suitable as the emissive center for the simplicity in discussing $T_1 \rightarrow Yb(^2F_{5/2})$ energy transfer process. Gd(III) and Lu(III) ions were chosen as the non-emissive paramagnetic and diamagnetic centers, respectively.

To investigate the effect of SOC strength induced by paramagnetic and diamagnetic Ln(III) ions on the PSET efficiency, we synthesized nonanuclear Yb_nGd_{9-n} and Yb_nLu_{9-n} clusters ($[Ln_9(\mu-OH)_{10}(\text{butyl salicylate})_{16}]NO_3$, Ln = Yb_nGd_{9-n} / Yb_nLu_{9-n} , $n = 0, 1, 3, 7, 9$). The clusters were identified with IR and mass spectroscopy as well as elemental analysis. The structural analysis was performed by the combination of powder and single-crystal XRD measurements. The effect of SOC was elucidated by emission spectra and lifetimes. We explore whether the PSET efficiency is reduced or raised in the presence of a strong SOC. Either result provides important insight into fundamental photophysics of Ln(III) complexes as well as factors to consider when designing them and to optimize the energy transfer efficiency.

2. Experimental section

2.1. Materials

$Gd(NO_3)_3 \cdot 6H_2O$ (> 99.95%) and $Lu(NO_3)_3 \cdot 4H_2O$ (> 99.95%) were purchased from Kanto Chemical Co., and $Yb(NO_3)_3 \cdot 5H_2O$ (99.9%) was purchased from Sigma-Aldrich Japan. Butylsalicylate was purchased from Tokyo Chemical Industries. Methanol for spectroscopy was purchased from Wako Pure Chemical Industries, Ltd. All reagents were used without further purification.

2.2. Characterization

FAB-MS and ESI-MS spectra were measured on a JEOL JMS-700TZ and JEOL JMS-T100LP, respectively. Elemental analyses were performed by Exter Analytical CE440. Infrared spectra were recorded on a JASCO FT/IR-4600 spectrometer. XRD spectra were characterized by a RIGAKU SmartLab X-ray diffractometer. Single crystal X-ray diffractions were made on a RIGAKU RAXIS RAPID imaging plate area detector.

2.3. Synthesis

Yb_nGd_{9-n} and Yb_nLu_{9-n} clusters were synthesized following the procedures previously reported.[15]

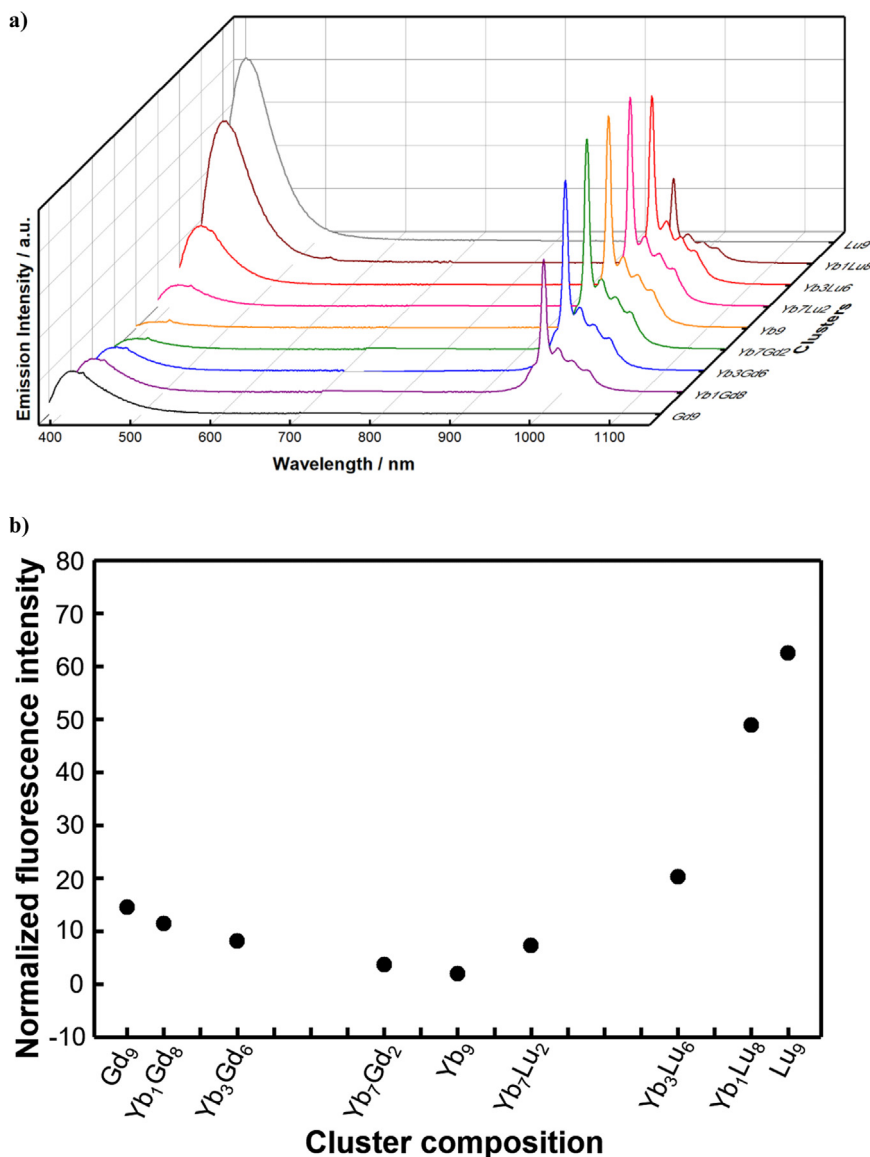


Fig. 3. a) Emission spectra of degassed $\text{Yb}_n\text{Gd}_{9-n} / \text{Yb}_n\text{Lu}_{9-n}$ clusters in 1.0×10^{-4} M methanol solution excited at 371 nm. b) The plot of fluorescence intensity normalized by the intensity of Yb_9 cluster.

Gd₉ cluster: Yield: 68%. Selected IR (ATR, cm^{-1}): 3573 (w, O–H), 3235 (w, O–H), 2956 (m, C–H), 1319 (s, C–O). FAB-MS: $m/z = 4676.8$ $[\text{Gd}_9(\mu\text{-OH})_{10}(\text{butylsalicylate})_{16}]^+$. Elemental analysis calculated for $\text{C}_{176}\text{H}_{218}\text{NO}_{61}\text{Gd}_9$: C, 44.61%, H, 4.64%, N, 0.30%. Found: C, 44.30%, H, 4.53%, N, < 0.30%.

Yb₁Gd₈ cluster: Yield: 67%. Selected IR (ATR, cm^{-1}): 3572 (w, O–H), 3235 (w, O–H), 2957 (m, C–H), 1319 (s, C–O). FAB-MS: $m/z = 4692.2$ $[\text{Yb}_1\text{Gd}_8(\mu\text{-OH})_{10}(\text{butylsalicylate})_{16}]^+$. Elemental analysis calculated for $\text{C}_{176}\text{H}_{218}\text{NO}_{61}\text{Yb}_1\text{Gd}_8$: C, 44.46%, H, 4.62%, N, 0.29%. Found: C, 43.98%, H, 4.45%, N, < 0.30%.

Yb₃Gd₆ cluster: Yield: 78%. Selected IR (ATR, cm^{-1}): 3572 (w, O–H), 3223 (w, O–H), 2957 (m, C–H), 1319 (s, C–O). FAB-MS: $m/z = 4724.3$ $[\text{Yb}_3\text{Gd}_6(\mu\text{-OH})_{10}(\text{butylsalicylate})_{16}]^+$. Elemental analysis calculated for $\text{C}_{176}\text{H}_{218}\text{NO}_{61}\text{Yb}_3\text{Gd}_6$: C, 44.17%, H, 4.59%, N, 0.29%. Found: C, 43.77%, H, 4.41%, N, < 0.30%.

Yb₇Gd₂ cluster: Yield: 85%. Selected IR (ATR, cm^{-1}): 3582 (w, O–H), 3210 (w, O–H), 2957 (m, C–H), 1321 (s, C–O). FAB-MS: $m/z = 4785.8$ $[\text{Yb}_7\text{Gd}_2(\mu\text{-OH})_{10}(\text{butylsalicylate})_{16}]^+$. Elemental analysis calculated for $\text{C}_{176}\text{H}_{218}\text{NO}_{61}\text{Yb}_7\text{Gd}_2$: C, 43.59%, H, 4.53%, N, 0.29%. Found: C, 43.27%, H, 4.36%, N, < 0.30%.

Yb₉ cluster: Yield: 78%. Selected IR (ATR, cm^{-1}): 3585 (w, O–H),

3206 (w, O–H), 2956 (m, C–H), 1320 (s, C–O). FAB-MS: $m/z = 4819.0$ $[\text{Yb}_9(\mu\text{-OH})_{10}(\text{butylsalicylate})_{16}]^+$. Elemental analysis calculated for $\text{C}_{176}\text{H}_{218}\text{NO}_{61}\text{Yb}_9$: C, 43.31%, H, 4.50%, N, 0.29%. Found: C, 42.99%, H, 4.37%, N, < 0.30%.

Yb₇Lu₂ cluster: Yield: 80%. Selected IR (ATR, cm^{-1}): 3585 (w, O–H), 3226 (w, O–H), 2956 (m, C–H), 1321 (s, C–O). ESI-MS: $m/z = 4822.74$ $[\text{Yb}_7\text{Lu}_2(\mu\text{-OH})_{10}(\text{butylsalicylate})_{16}]^+$. Elemental analysis calculated for $\text{C}_{176}\text{H}_{218}\text{NO}_{61}\text{Yb}_7\text{Lu}_2$: C, 43.27%, H, 4.50%, N, 0.29%. Found: C, 42.94%, H, 4.37%, N, < 0.30%.

Yb₃Lu₆ cluster: Yield: 28%. Selected IR (ATR, cm^{-1}): 3584 (w, O–H), 3206 (w, O–H), 2957 (m, C–H), 1321 (s, C–O). ESI-MS: $m/z = 4830.73$ $[\text{Yb}_3\text{Lu}_6(\mu\text{-OH})_{10}(\text{butylsalicylate})_{16}]^+$. Elemental analysis calculated for $\text{C}_{176}\text{H}_{218}\text{NO}_{61}\text{Yb}_3\text{Lu}_6$: C, 43.21%, H, 4.49%, N, 0.29%. Found: C, 42.73%, H, 4.31%, N, 0.25%.

Yb₁Lu₈ cluster: Yield: 81%. Selected IR (ATR, cm^{-1}): 3586 (w, O–H), 3208 (w, O–H), 2956 (m, C–H), 1321 (s, C–O). ESI-MS: $m/z = 4834.75$ $[\text{Yb}_1\text{Lu}_8(\mu\text{-OH})_{10}(\text{butylsalicylate})_{16}]^+$. Elemental analysis calculated for $\text{C}_{176}\text{H}_{218}\text{NO}_{61}\text{Yb}_1\text{Lu}_8$: C, 43.17%, H, 4.49%, N, 0.29%. Found: C, 43.04%, H, 4.36%, N, < 0.30%.

Lu₉ cluster: Yield: 80%. Selected IR (ATR, cm^{-1}): 3586 (w, O–H), 3207 (w, O–H), 2957 (m, C–H), 1321 (s, C–O). FAB-MS: m/z

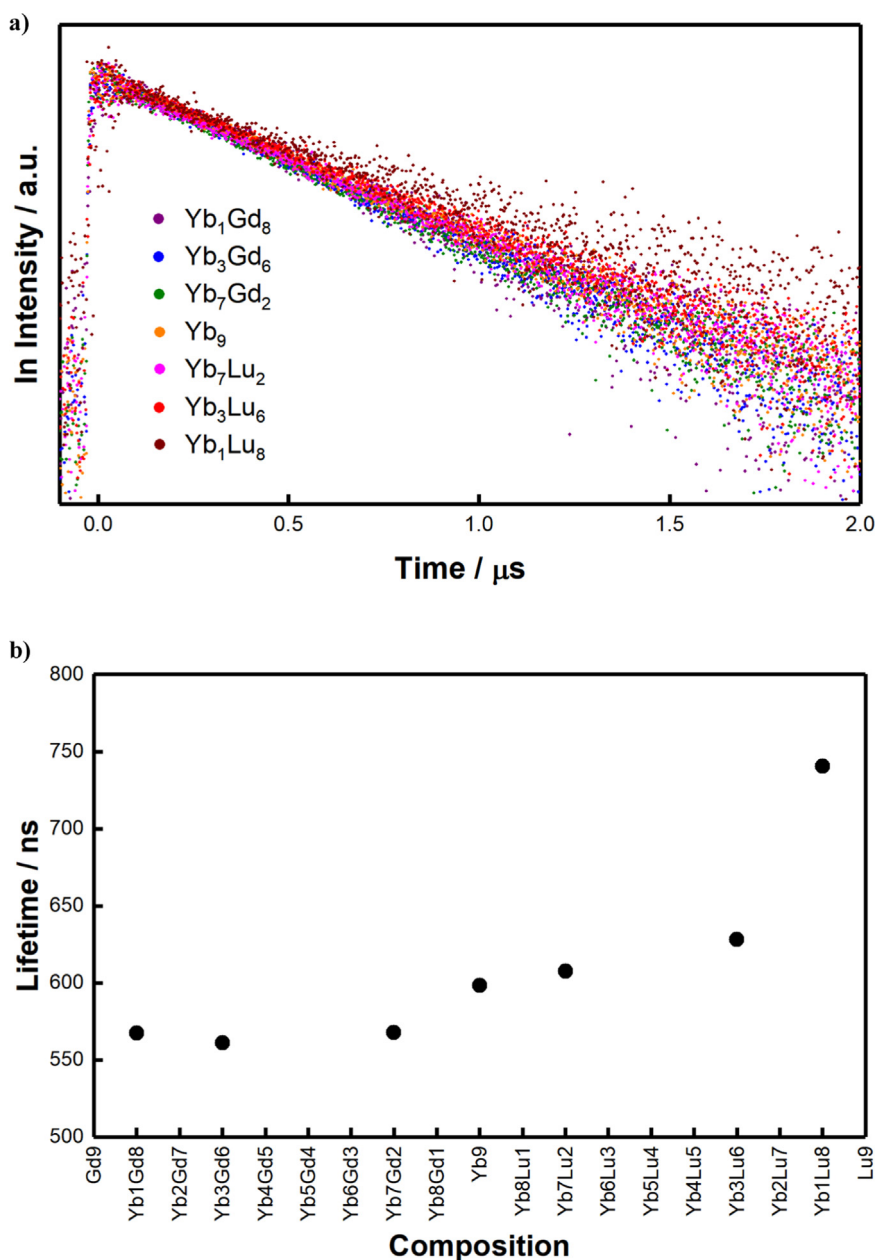


Fig. 4. a) Normalized emission decay profiles of degassed $\text{Yb}_n\text{Gd}_{9-n} / \text{Yb}_n\text{Lu}_{9-n}$ clusters in 1.0×10^{-4} M methanol solution excited at 371 nm and monitored at 976 nm (Yb(III) emission). b) The plot of emission lifetimes of the clusters derived from the single-exponential fitting of the decay profiles.

$z = 4836.1$ $[\text{Lu}_9(\mu\text{-OH})_{10}(\text{butylsalicylate})_{16}]^+$. Elemental analysis calculated for $\text{C}_{176}\text{H}_{218}\text{NO}_{61}\text{Lu}_9$: C, 43.16%, H, 4.49%, N, 0.29%. Found: C, 42.82%, H, 4.33%, N, < 0.30%.

2.4. Spectroscopy

Absorption spectra of the clusters were obtained by using a JASCO V-670 spectrometer. Emission spectra and lifetimes were measured using a Horiba/Jobin-Yvon FluoroLog-3 ps spectrofluorometer. The emission spectra of UV–vis and NIR region were connected using Eu(hfa)₃(TPPO)₂ complex [16] as a reference to match the detection level of both detectors. A combination of JASCO FP-6600 spectrometer and Oxford Instruments OptistatDN2 cryostat was used to measure emission spectra at low temperature. The absolute quantum yield were measured by a combination of JASCO FP-6600 and an integration sphere.

3. Results and discussion

3.1. Characterization

The crystal structures of Yb_9 cluster are shown in Fig. 2. Continuous shape measure analysis was employed for the Yb(III) ions in the clusters to investigate the coordination geometry (see Supplementary Information for the method). [17] The results summarized in Table 1 confirm that there are eight 8-coordinated trigonal dodecahedron and one 8-coordinated square antiprism coordination sites for Yb(III) ions in Yb_9 clusters. Lu_9 cluster (Fig. S1b) and the previously reported Gd_9 clusters [15] have a similar structure as the Yb_9 clusters. As a crystal, these three clusters have different crystal system with Yb_9 and Lu_9 clusters being triclinic while Gd_9 being orthorhombic. This may be due to the larger ionic radii of Gd(III) ions. To compare the structure of the other clusters ($\text{Yb}_n\text{Gd}_{9-n}$ and $\text{Yb}_n\text{Lu}_{9-n}$, $n = 1, 3$, and 7), XRD measurements were performed. The XRD patterns for the clusters shown in

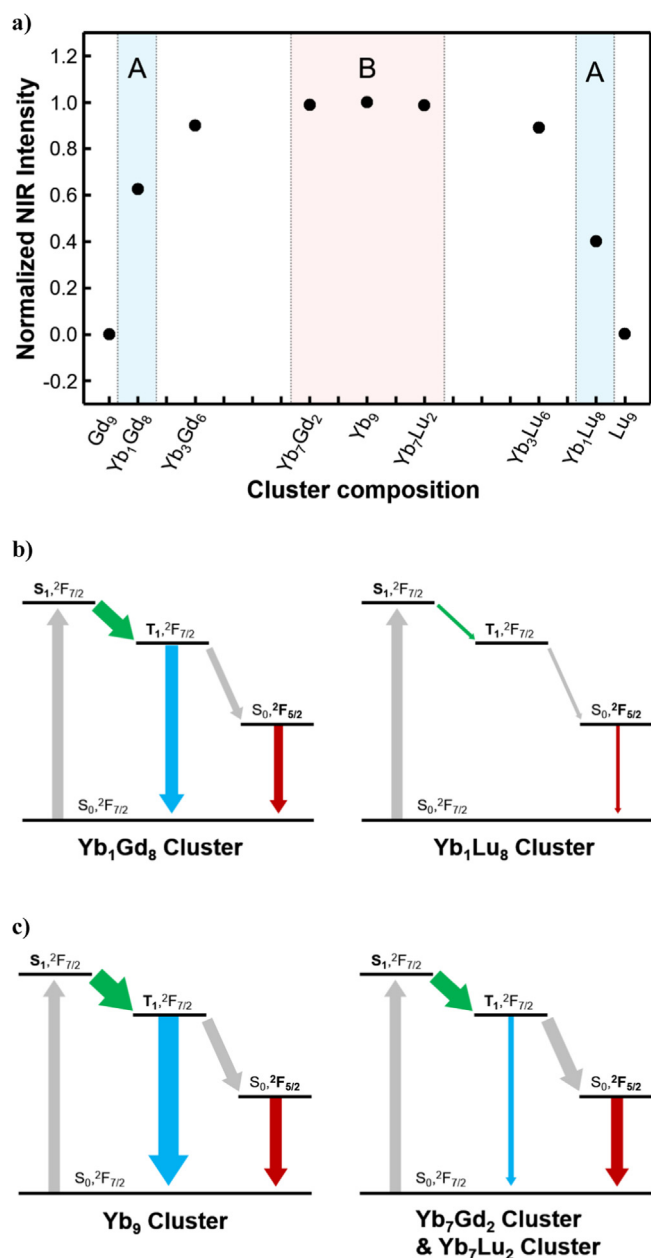


Fig. 5. a) Plot of the peak of NIR emission intensity normalized by the intensity of Yb₉ cluster. The shaded area represents two different regions (A and B) in which the dominating photophysical process differs. b) Comparison of the photophysical processes in Yb₁Gd₈ and Yb₁Lu₈ clusters (region A), and c) Yb₉, Yb₇Lu₂, Yb₇Gd₂ clusters (region B). The thickness of the arrows represents the yield resulting from the process (not the rate constant of the process).

Fig. S2 are similar, but the peaks shift to lower angle with increasing number of Yb(III) and Lu(III) ions compared to Gd₉ cluster. It should be noted that the spectroscopic measurements were performed in methanol solution, and thus intermolecular interaction is minimized. Any spectroscopic differences of the clusters arise from the structure of a single molecule. This will become important for the later discussion because distortion of ligand alignment may affect both the ligand and Yb(III) emission.

3.2. Spectroscopic results

The emission intensity of the fluorescence and phosphorescence from the ligands in Yb_nGd_{9-n} and Yb_nLu_{9-n} clusters provides information

on photophysical properties of the ligands (i.e., SOC) under the influence of the paramagnetic effect of Ln(III) ions. On the other hand, the emission intensity of Yb(III) emission implies the efficiency of PSET. The emission spectra of Yb_nGd_{9-n} and Yb_nLu_{9-n} clusters in 1.0×10^{-4} M methanol solution (degassed) in the visible and NIR region excited at 371 nm are shown in Fig. 3a. The peak at 410 nm corresponds to the fluorescence from the butyl salicylate ligands. The fluorescence intensity is the lowest for Yb₉ clusters and increases with increasing number of Gd(III) or Lu(III) ions. Increasing the number of Lu(III) ions showed greater enhancement in emission intensity compared with Gd(III) ions (Fig. 3b). Since SOC enhances the S₁ → T₁ ISC rates, which reduces the quantum yield of fluorescence from the ligands, the strength of SOC in this cluster is in the order of Yb(III) > Gd(III) > Lu(III). A similar trend was reported by Guldi. [13] The absolute quantum yield of the fluorescence of Lu₉ cluster was below 1% (calculated as 0.2%). Phosphorescence was observed at low temperature (180 K) for Gd₉ and Yb₉ clusters at around 465 nm (Fig. S3). The intensity of the phosphorescence in relative to the fluorescence is significantly reduced for Yb₉ clusters due to the presence of T₁ → Ln energy transfer. Phosphorescence was not observed for Lu₉ clusters because of the high fluorescence intensity, and low S₁ → T₁ ISC and T₁ → S₀ relaxation rate compared to those of Gd₉ clusters.

The emission peak at 976 nm in Fig. 3a originates from the ²F_{5/2} → ²F_{7/2} transition of Yb(III) ions. The spectral shape of the Yb(III) near-infrared (NIR) emission was identical for all compositions. The spectral shape of Ln(III) emission is known to be sensitive to the coordination geometry, [9,18,19] thus the NIR emission spectra show that the coordination geometries around Yb(III) ions are identical for all clusters. The continuous shape measure calculation (see Section 3.1) supports this analysis. Based on the identical local coordination geometry, the radiative rate constant of Yb(III) ions in these clusters is expected to be equal.

The NIR emission lifetimes monitored at 976 nm ($\lambda_{\text{EX}} = 976$ nm) were single-component for all compositions (Fig. 4a). Single-exponential fit showed that the emission lifetimes of the clusters gradually increased with decreasing number of Gd(III) ions and increasing number of Lu(III) ions (Fig. 4b). In particular, the emission lifetimes of Yb₁Gd₈, Yb₉, and Yb₁Lu₈ clusters were 568, 598, and 740 ns. The short lifetimes indicate large nonradiative rate constant and thus the emission quantum yield of Yb(III) ions in these clusters are likely below 1%. The lifetimes are similar and the small variation may be due to differences in the ionic radii of Gd(III), Yb(III), and Lu(III) ions leading to differences in the values of nonradiative rate constants of Yb(III) ions in the clusters.

Fig. 5a shows the plot of the NIR emission intensity of the clusters, normalized by the intensity of Yb₉ cluster. The emission intensities in the plot represent the PSET efficiency of the clusters. The intensity of Yb₁Gd₈ cluster was 1.6 times higher than that of Yb₁Lu₈ cluster. For these two clusters (region A of Fig. 5a), the SOC induced by Gd(III) or Lu(III) ions contributed to the difference in the S₁ → T₁ ISC efficiency. Stronger SOC by Gd(III) ions leads to more efficient S₁ → T₁ ISC (Fig. 5b, green arrow) in Yb₁Gd₈ cluster compared to that of Yb₁Lu₈ cluster and explains the higher Yb³⁺ NIR emission intensity. On the other hand, Yb₇Gd₂ and Yb₇Lu₂ clusters showed the same emission intensity as Yb₉ clusters (region B of Fig. 5a). Normally, reduced number of emissive Ln(III) ions leads to a decrease in T₁ → Ln energy transfer efficiencies but this was not observed. Thus, the mixture of Gd(III) and Lu(III) ions reduced the T₁ → S₀ relaxation (Fig. 5c, blue arrow), which compensated for the reduced number of Yb(III) ions. These results suggest that there is an optimal strength of SOC for a high PSET efficiency in Ln(III) complexes.

4. Conclusions

In this study, the effect of SOC strength induced by paramagnetic and diamagnetic Ln(III) ions on the PSET efficiency in nonanuclear Ln

(III) clusters was explored. We have synthesized nonanuclear $\text{Yb}_n\text{Gd}_{9-n}$ and $\text{Yb}_n\text{Lu}_{9-n}$ clusters ($[\text{Ln}_9(\mu\text{-OH})_{10}(\text{butyl salicylate})_{16}]\text{NO}_3$, $\text{Ln} = \text{Yb}_n\text{Gd}_{9-n} / \text{Yb}_n\text{Lu}_{9-n}$, $n = 0, 1, 3, 7, 9$) and investigated their photophysical properties by emission spectra and lifetimes. The result reveal that SOC affects the PSET efficiency both positively and negatively depending on the strength of SOC, and thus there is an optimal region in the SOC strength. We also suggest that mixing Ln(III) ions with different SOC in Ln(III) clusters is an effective method to optimize PSET efficiency. The findings are another step forward in understanding the fundamental photophysical processes in Ln(III) complexes, as well as providing a possible novel strategy to enhance the luminescence efficiency.

Acknowledgement

This work was partly supported by the Ministry of Education, Science, Sports and Culture, Grant-in-Aid for Young Scientists (A), 17H04873, 2017, and Grant-in-Aid for JSPS Fellows, 16J0130507, 2017. We also thank Dr. Hiroyasu Sato of RIGAKU Corporation for single-crystal X-ray analyses of Yb_9 and Lu_9 clusters.

Appendix A. Supplementary material

Supplementary data associated with this article can be found in the online version at [doi:10.1016/j.jlumin.2018.04.049](https://doi.org/10.1016/j.jlumin.2018.04.049).

References

- [1] P.P. Lima, F.A.A. Paz, C.D.S. Brites, W.G. Quirino, C. Legnani, M.C.E. Silva, R.A.S. Ferreira, S.A. Júnior, O.L. Malta, M. Cremona, L.D. Carlos, White OLED based on a temperature sensitive $\text{Eu}^{3+}/\text{Tb}^{3+}/\beta\text{-diketonate}$ complex, *Org. Electron.* 15 (2014) 798–808.
- [2] I.V. Taydakov, A.A. Akkuzina, R.I. Avetisov, A.V. Khomyakov, R.R. Saifutayarov, I.C. Avetisov, Effective electroluminescent materials for OLED applications based on lanthanide 1,3-diketones bearing pyrazole moiety, *J. Lumin.* 177 (2016) 31–39.
- [3] D.T. Thielemann, A.T. Wagner, E. Roesch, D.K. Koelmel, J.G. Heck, B. Rudat, M. Neumaier, C. Feldmann, U. Schepers, S. Bräse, P.W. Roesky, Luminescent cell-penetrating pentadecanuclear lanthanide clusters, *J. Am. Chem. Soc.* 135 (2013) 7454–7457.
- [4] T. Zhang, X. Zhu, C.C.W. Cheng, W.-M. Kwok, H.-L. Tam, J. Hao, D.W.J. Kwong, W.-K. Wong, K.-L. Wong, Water-soluble mitochondria-specific ytterbium complex with impressive NIR emission, *J. Am. Chem. Soc.* 133 (2011) 20120–20122.
- [5] S. Marchionna, F. Meinardi, M. Acciarri, S. Binetti, A. Papagni, S. Pizzini, V. Malatesta, R. Tubino, Photovoltaic quantum efficiency enhancement by light harvesting of organo-lanthanide complexes, *J. Lumin.* 118 (2006) 325–329.
- [6] H. Kataoka, T. Kitano, T. Takizawa, Y. Hirai, T. Nakanishi, Y. Hasegawa, Photo- and thermo-stable luminescent beads composed of $\text{Eu}(\text{III})$ complexes and PMMA for enhancement of silicon solar cell efficiency, *J. Alloy. Compd.* 601 (2014) 293–297.
- [7] E.G. Moore, A.P.S. Samuel, K.N. Raymond, From antenna to assay: lessons learned in lanthanide luminescence, *Acc. Chem. Res.* 42 (2009) 542–552.
- [8] C. Huang, *Rare Earth Coordination Chemistry: Fundamentals and Applications*, John Wiley & Sons Pte. Ltd., 2010.
- [9] N.B.D. Lima, S.M.C. Gonçalves, S.A. Júnior, A.M. Simas, A comprehensive strategy to boost the quantum yield of luminescence of europium complexes, *Sci. Rep.* 3 (2013) 2395.
- [10] L.S. Forster, Intersystem crossing in transition metal complexes, *Coord. Chem. Rev.* 250 (2006) 2023–2033.
- [11] S. Tobita, M. Arakawa, I. Tanaka, The paramagnetic metal effect on the ligand localized S1-T1 intersystem crossing in the rare-earth-metal complexes with methyl salicylate, *J. Phys. Chem.* 89 (1985) 5649–5654.
- [12] S. Tobita, M. Arakawa, I. Tanaka, Electronic relaxation processes of rare earth chelates of benzoyltrifluoroacetone, *J. Phys. Chem.* 88 (1984) 2697–2702.
- [13] D.M. Guldi, T.D. Mody, N.N. Gerasimchuk, D. Magda, J.L. Sessler, Influence of large metal cations on the photophysical properties of texaphyrin, a rigid aromatic chromophore, *J. Am. Chem. Soc.* 122 (2000) 8289–8298.
- [14] T. Nakanishi, Y. Suzuki, Y. Doi, T. Seki, H. Koizumi, K. Fushimi, K. Fujita, Y. Hinatsu, H. Ito, K. Tanaka, Y. Hasegawa, Enhancement of optical faraday effect of nonanuclear $\text{Tb}(\text{III})$ complexes, *Inorg. Chem.* 53 (2014) 7635–7641.
- [15] S. Omagari, T. Nakanishi, Y. Kitagawa, T. Seki, K. Fushimi, H. Ito, A. Meijerink, Y. Hasegawa, Critical role of energy transfer between terbium ions for suppression of back energy transfer in nonanuclear terbium clusters, *Sci. Rep.* 6 (2016) 37008.
- [16] Y. Hasegawa, M. Yamamuro, Y. Wada, N. Kanehisa, Y. Kai, S. Yanagida, Luminescent polymer containing the $\text{Eu}(\text{III})$ complex having fast radiation rate and high emission quantum efficiency, *J. Phys. Chem. A* 107 (2003) 1697–1702.
- [17] M. Pinsky, D. Avnir, Continuous symmetry measures. 5. the classical polyhedra, *Inorg. Chem.* 37 (1998) 5575–5582.
- [18] Y. Hasegawa, T. Ohkubo, T. Nakanishi, A. Kobayashi, M. Kato, T. Seki, H. Ito, K. Fushimi, Effect of ligand polarization on asymmetric structural formation for strongly luminescent lanthanide complexes, *Eur. J. Inorg. Chem.* (2013) 5911–5918.
- [19] K. Miyata, T. Nakagawa, R. Kawakami, Y. Kita, K. Sugimoto, T. Nakashima, T. Harada, T. Kawai, Y. Hasegawa, Remarkable luminescence properties of lanthanide complexes with asymmetric dodecahedron structures, *Chem. Eur. J.* 17 (2011) 521–528.